arXiv:1011.4373v2 [physics.comp-ph] 24 Feb 2011

# A symplectic, symmetric algorithm for spatial evolution of particles in a time-dependent field☆

A. Ruzzon[a,b], Y. Elskens[a,*], F. Doveil[a]

[a] *Equipe turbulence plasma, case 321, PIIM, UMR 6633 CNRS – Aix-Marseille université, campus Saint-Jérôme, FR-13397 Marseille cedex 13*
[b] *Consorzio RFX, Corso Stati Uniti 4, IT-35127 Padova, Italy*

**Abstract**

A symplectic, symmetric, second-order scheme is constructed for particle evolution in a time-dependent field with a fixed spatial step. The scheme is implemented in one space dimension and tested, showing excellent adequacy to experiment analysis.

*Keywords:* symplectic integrator, wave-particle interaction, hamiltonian chaos, resonance overlap, traveling wave tube
*PACS:* 52.65.Cc, 05.45.Pq, 41.75.-i, 05.45.Ac, 52.65.Yy, 02.70.Ns, 52.20.Dq

## 1. Introduction

Particle motion in a space-time dependent field is a classical fundamental problem of dynamics. It is generally well solved in most settings under most kinds of requirements. However, most solutions deal with formulations of the dynamics where the independent variable is time, viz. they aim at computing a function $y$ such that the motion reads $x = y(t)$. Yet in some settings one actually describes motion by the reciprocal function $\tau = y^{-1}$, so that the motion reads $t = \tau(x)$.

One such instance is the propagation of electrons in a traveling wave tube, where it is natural to record particles when they pass at a fixed probe location, instead

☆©2011 The authors. Reproduction of this article, in its entirety, for noncommercial purposes is permitted.

*corresponding author
*Email addresses:* alberto.ruzzon@igi.cnr.it (A. Ruzzon), yves.elskens@univ-provence.fr (Y. Elskens), fabrice.doveil@univ-provence.fr (F. Doveil)

of getting a snapshot of their locations at a given time. Similar physical contexts are met in other particle beam devices, such as accelerators, klystrons, free electron lasers, electronic tubes for wave amplification,...[14] To some extent, this description is somewhat analogous to eulerian descriptions of flows in hydrodynamics.

If one were interested in the evolution of a single particle, one could merely compute its motion as $x = y(t)$ and deduce its "schedule" function $t = \tau(x)$ and related quantities as functions of spatial position. In this respect, many symplectic methods are available (see e.g. Refs [12, 15] for an overview), especially for separable hamiltonians of the form $H(p, x, t) = K(p) + V(x, t)$. However, to describe a beam of many particles during their spatial progression, it is reasonable to follow them consistently in space, to generate numerical data sampled at the same (possibly many) space positions. It then becomes awkward to first evolve them in time and afterwards reconstruct their progression in spatial terms by interpolations.

For this purpose we reformulate in Section 2 the particle equations of motion, using the streaming variable $x$ as independent variable (see figure 1). Since the original particle dynamics is hamiltonian, we ensure that the new description be symplectic by first expressing the action principle in terms of the timetable function $\tau$. In the corresponding hamiltonian picture, the variable conjugate to $\tau$ is the energy $\zeta$, and the generator of motion is momentum $\mathcal{P}$.

In Section 3 we stress our requirements on the scheme and consider alternative strategies. Then we construct a first order symplectic scheme for the particle motion. The implicit part of the step can be performed either through algebraic solution of a cubic equation, or through a Newton iteration : we compare both procedures. Next we construct the adjoint, first order symplectic scheme, which also requires a Newton iteration, and we check its accuracy. Finally, we combine the direct and adjoint schemes to obtain a second order symmetric, symplectic, fixed $\Delta x$ scheme.

In Section 4 we benchmark our algorithm by analysing the particle motion in the field of a single harmonic wave, viz. we solve the pendulum motion in a galilean frame. Numerical simulations for realistic beam data generate beam deformations shown in Section 5.

Section 6 focuses on the evolution of a beam launched in presence of two harmonic waves. Simulations are confronted with experimental observations of the beam collected at the device outlet. Special attention is paid to the reproduction of a devil staircase structure, characteristic of the chaotic behaviour of the system, taking into account the finiteness of the experimental device.

In summary, experimental data often relate to limited interaction times, while

numerical evidences and theoretical discussions of chaotic dynamics often deal with trajectories followed for long times in a compact domain of phase space. The agreement of our simulations with experimental evidence assesses the relevance of our algorithm to such experimental settings.

## 2. Evolution with respect to space

Rewriting the equations of motion in hamiltonian form with respect to space is straightforward in the symplectic formalism (see Section 2.2). However one may wish first a more pedestrian derivation, from the classical action principle.

### *2.1. Lagrangian viewpoint*

The action for a non-relativistic particle with mass $m$ moving along a one-dimensional axis O$x$ in a time dependent potential $V(x,t)$ reads

$$S[y;t_0,t_1,x_0,x_1]=\int_{t_0}^{t_1}L(y(t),\dot{y}(t),t)\mathrm{d}t \tag{1}$$

where $y$ is a continuously differentiable function of time $t\in[t_0,t_1]\subset\mathbb{R}$, subject to the constraints $y(t_0)=x_0$ and $y(t_1)=x_1$, and the dot denotes derivative with respect to $t$. The lagrangian is

$$L(x,v,t)=\frac{mv^2}{2}-V(x,t)\,. \tag{2}$$

In the following we restrict all trajectories to the class of strictly monotone, increasing functions, viz. $\inf_{t_0<t<t_1}\dot{y}(t)>0$. For these functions the reciprocal function $\tau:[x_0,x_1]\to[t_0,t_1]:x\mapsto\tau(x)$ exists ; $\tau$ is unique and also strictly monotone, increasing, continuously differentiable with

$$\tau'(x)=\frac{\mathrm{d}\tau}{\mathrm{d}x}(x)=\left(\frac{\mathrm{d}y}{\mathrm{d}t}(\tau(x))\right)^{-1}=\frac{1}{\dot{y}(\tau(x))} \tag{3}$$

where the prime denotes derivative with respect to $x$.

To rewrite (1) as a space-integral, we introduce the new lagrangian

$$\mathcal{L}(t,u,x):=L(x,\frac{1}{u},t)u \tag{4}$$

so that

$$\mathcal{S}[\tau;x_0,x_1,t_0,t_1]:=S[\tau^{-1};t_0,t_1,x_0,x_1]=\int_{x_0}^{x_1}\mathcal{L}(\tau(x),\tau'(x),x)\mathrm{d}x\,. \tag{5}$$

It is convenient to introduce the opposite to the (usual definition of) canonical momentum conjugate to $\tau$,

$$\zeta = -\frac{\partial \mathcal{L}}{\partial u} \tag{6}$$

and to perform the Legendre transform of $-\mathcal{L}$, defining

$$\mathcal{P}(\zeta, t, x) := \zeta\tau' + \mathcal{L}(t, \tau', x) \tag{7}$$

so that in the new variables the canonical Hamilton equations read

$$\frac{\mathrm{d}\tau}{\mathrm{d}x} = \frac{\partial \mathcal{P}}{\partial \zeta}, \tag{8}$$

$$\frac{\mathrm{d}\zeta}{\mathrm{d}x} = -\frac{\partial \mathcal{P}}{\partial \tau}. \tag{9}$$

For the classical lagrangian (2) the new variables are the usual energy and linear momentum,

$$\zeta = \frac{m}{2\tau'^2} + V(x, \tau(x)), \tag{10}$$

$$\mathcal{P} = \sqrt{2m(\zeta - V(x, \tau(x)))}. \tag{11}$$

*2.2. Hamiltonian viewpoint*

The hamiltonian formulation of dynamics provides a direct path to the latter equations. Indeed it suffices to consider the symplectic 2-form

$$\mathrm{d}\omega := \mathrm{d}p\mathrm{d}x - \mathrm{d}H\mathrm{d}t \tag{12}$$

where $p = m\dot{y}$ is conjugate to $x$ and $H = \zeta$ is conjugate to $t = \tau$, and to consider $x$ as the independent variable along trajectories instead of $t$. The minus sign we introduced in (6)-(7) ensures the usual signs in $\mathrm{d}\omega$.

Of course, if the potential does not depend explicitly on time, $\zeta$ is a first integral.

The above requirement, that $\dot{y}$ nowhere vanishes, will be strengthened below by imposing $\mathcal{P} \geq p_{\min} > 0$ for some $p_{\min}$ to ensure appropriate numerical accuracy.

## 3. Discrete time canonical transformations

To preserve the symplectic structure while integrating (10)-(11) we use a sequence of canonical transformations. Note that (11) does not allow using a splitting method such as leap-frog [12, 15], as it is not the sum of integrable generators.

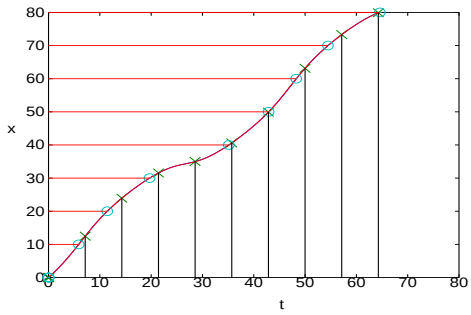


Figure 1: Sketch of the algorithm principle in $(x, t)$ plot. The continued line is a trajectory (identical for both schemes, with small steps). Crosses sample positions (every $50\Delta t$) as obtained by leap-frog with constant time step, circles sample times (every $50\Delta x$) as obtained by our approach with constant space step. Straight lines are guides to the eye.

In order to sample the spatial evolution regularly (as desired e.g. to follow many particles in parallel), we use a fixed spatial step $\Delta x$, a strategy recommended e.g. by Hénon [13] to obtain simple and accurate Poincaré maps (for a space periodic potential, the step $\Delta x$ is best taken as a fraction of the wavelength). A fixed spatial step also avoids generating noisy-like "spurious frequencies" in the simulated dynamics. Note that we could also use a time-integrator (leap-frog or other) with an adapting time step, $\Delta t = m\Delta x/\mathcal{P}$ [13], but it is not manifestly symplectic as $\mathcal{P}$ is not constant. Another approach, using a fixed time step and interpolating the trajectories for the spatial mesh, would raise the issue of constructing a symplectic interpolation scheme (of desired order). In this work we settle for the manifestly symplectic, fixed step approach, which can process many particles in parallel.

Our first integrator $\mathcal{F}_{\Delta x} : (\tau, \zeta, x) \mapsto (\tilde{\tau}, \tilde{\zeta}, x + \Delta x)$ is chosen to provide an explicit, first-order approximation for the time increment. It is generated by

$$F(\tau, \tilde{\zeta}) = \tau\tilde{\zeta} + \mathcal{P}(\tau, \tilde{\zeta}, x)\Delta x \tag{13}$$

so that the system

$$\zeta = \tilde{\zeta} + \partial_\tau \mathcal{P}(\tau, \tilde{\zeta}, x)\Delta x\,, \tag{14}$$
$$\tilde{\tau} = \tau + \partial_{\tilde{\zeta}} \mathcal{P}(\tau, \tilde{\zeta}, x)\Delta x\,, \tag{15}$$

is a first-order, symplectic approximation to (8)-(9). As the second equation is explicit with respect to time $\tilde{\tau}$, the first equation is implicit with respect to the energy $\tilde{\zeta}$. For

the special case of momentum (11), it actually leads to a cubic equation,

$$\tilde{\zeta}^3 - (V + 2\zeta)\tilde{\zeta}^2 + (2V\zeta + \zeta^2)\tilde{\zeta} - V\zeta^2 - \frac{m}{2}(\partial_\tau V)^2 \Delta x^2 = 0\,, \tag{16}$$

which can be solved algebraically for $\tilde{\zeta}$. Here $V$ and $\partial_\tau V$ are computed at $(x, \tau)$. Equation (16) usually has three real solutions, two of which being $\Delta x$-close to $\zeta$ : the relevant root is such that $(\zeta - \tilde{\zeta})\,\partial_\tau V > 0$.

It is advantageous to express (14) in the form $\tilde{\zeta} = \zeta + (\zeta - V)\sigma$, so that

$$\sigma = -a\,(1 + \sigma)^{-1/2} \tag{17}$$

with the single parameter

$$a = \sqrt{m/2}\,(\zeta - V)^{-3/2}\,\partial_\tau V \Delta x \tag{18}$$

calculated at $(x, \tau)$. The fixed point equation (17) is easily solved by the Newton method, which selects the "good" cubic root automatically (as $a\sigma < 0$) and converges very fast, especially if $a$ is small. Analytically, this method stresses the small parameter $a$ controlling the accuracy of our scheme : it involves a balance of the potential evolution $\partial_\tau V$ and the spatial step $\Delta x$ against $(\zeta - V)$, viz. against the particle velocity $\mathcal{P}/m$. For small velocity, the algorithm deteriorates – at worst it will miss turning points where $\mathcal{P}$ changes sign (which is forbidden by our assumptions on trajectories in the action principle).

Let $\mathcal{Z}^{\rm C}_{\Delta x} : (\tau, \zeta, x) \mapsto (\tau, \tilde{\zeta}, x)$ and $\mathcal{Z}^{\rm N}_{\Delta x} : (\tau, \zeta, x) \mapsto (\tau, \tilde{\zeta}, x)$ denote respectively the cubic and Newton solvers. For perfectly accurate computations, they coincide and may be denoted identically $\mathcal{Z}_{\Delta x}$. Note that $\mathcal{Z}_{\Delta x}$ is not symplectic, as

$$\det D\mathcal{Z}_{\Delta x}(\tau, \zeta, x) = [1 + \partial_\zeta \partial_\tau \mathcal{P}(\tau, \tilde{\zeta}, x)\Delta x]^{-1}\,. \tag{19}$$

With the new energy $\tilde{\zeta}$, (15) immediately provides the new time, defining the map $\mathcal{T}_{\Delta x} : (\tau, \tilde{\zeta}, x) \mapsto (\tilde{\tau}, \tilde{\zeta}, x)$. This map is not symplectic either, as

$$\det D\mathcal{T}_{\Delta x}(\tau, \tilde{\zeta}, x) = 1 + \partial_\zeta \partial_\tau \mathcal{P}(\tau, \tilde{\zeta}, x)\Delta x\,. \tag{20}$$

Finally, we advance position, with $\mathcal{I}_{\Delta x} : (\tau, \zeta, x) \mapsto (\tau, \zeta, x + \Delta x)$. The resulting integration scheme $\mathcal{F}_{\Delta x} = \mathcal{I}_{\Delta x} \circ \mathcal{T}_{\Delta x} \circ \mathcal{Z}_{\Delta x}$ is symplectic by construction, within machine accuracy, as the planar map $\mathcal{T}_{\Delta x} \circ \mathcal{Z}_{\Delta x}$ is area-preserving : $\det D(\mathcal{T}_{\Delta x} \circ \mathcal{Z}_{\Delta x}) = (\det D\mathcal{T}_{\Delta x})(\det D\mathcal{Z}_{\Delta x}) = 1$. It is first order only.

| $v_{\rm in}$ | $\delta\zeta_{\rm estimate}$ | $\delta\zeta_{\rm simulation}$ | $\delta\tau_{\rm estimate}$ | $\delta\tau_{\rm simulation}$ |
|---|---|---|---|---|
| 2.5 | 0.16 | $6 \cdot 10^{-4}$ | 0.02 | 0.005 |
| 1.5 | 0.11 | $9 \cdot 10^{-4}$ | 0.10 | 0.03 |
| 0.9 | 0.10 | 0.008 | 8 | 0.5 |
| 0.6 | 20 | 0.1 | 12 | 5 |
| 0.4 | 3 | 0.3 | 70 | 16 |

Table 1: The largest single step error for five particles with different initial velocity launched in the field of a single wave with $A = 0.1$, $k = 0.2$, $v_\phi = 1$, $\phi = \pi/4$.

The variables advanced with (14) and (15) are in the form

$$\tilde{\tau} \quad \cong \quad \tau + \tau'\Delta x + \frac{\tau''}{2}\Delta x^2 + \mathrm{O}(\Delta x^3)\,, \tag{21}$$

$$\tilde{\zeta} \quad \cong \quad \zeta + \zeta'\Delta x + \frac{\zeta''}{2}\Delta x^2 + \mathrm{O}(\Delta x^3)\,, \tag{22}$$

where $\tau'$ and $\zeta'$ have been approximated with $-\partial_\tau \mathcal{P}(\tau, \tilde{\zeta}, x)$ and $\partial_\zeta \mathcal{P}(\tau, \tilde{\zeta}, x)$. It follows that the most influential theoretical error, in every step of integration, is given by $\tau''\Delta x/2$ for $\tilde{\tau}$ and $\zeta''\Delta x/2$ for $\tilde{\zeta}$. Table 1 compares the upper estimated theoretical errors, related to $\tau''$ and $\zeta''$, and the maximum real simulation errors for five particle initial velocities. Slower particles are found affected by larger errors as expected.

To obtain a second order, symmetric scheme, we consider the adjoint map [12], which is also symplectic, generated by the function

$$F^*(\tilde{\tau}, \zeta) = \tilde{\tau}\zeta - \mathcal{P}(\tilde{\tau}, \zeta, x + \Delta x)\Delta x \tag{23}$$

so that

$$\tau \;=\; \tilde{\tau} - \partial_\zeta \mathcal{P}(\tilde{\tau}, \zeta, x + \Delta x)\Delta x\,, \tag{24}$$

$$\tilde{\zeta} \;=\; \zeta - \partial_\tau \mathcal{P}(\tilde{\tau}, \zeta, x + \Delta x)\Delta x\,. \tag{25}$$

For momentum (11), both equations involve the potential $V(x + \Delta x, \tilde{\tau})$, which implies that one first solves (24) with respect to the new time $\tilde{\tau}$ by a Newton algorithm, and then computes the new energy $\tilde{\zeta}$ by (25). This defines the symplectic map $\mathcal{F}^*_{\Delta x} = \mathcal{Z}^*_{\Delta x} \circ \mathcal{T}^*_{\Delta x} \circ \mathcal{I}_{\Delta x} : (\tau, \zeta, x) \mapsto (\tilde{\tau}, \tilde{\zeta}, x + \Delta x)$.

One easily checks that $\mathcal{I}_{\Delta x}$ is self-adjoint, while $\mathcal{Z}^*_{\Delta x} \circ \mathcal{Z}_{-\Delta x}$ and $\mathcal{T}^*_{\Delta x} \circ \mathcal{T}_{-\Delta x}$ reduce to identity up to machine numerical tolerance (typically $10^{-15}$).

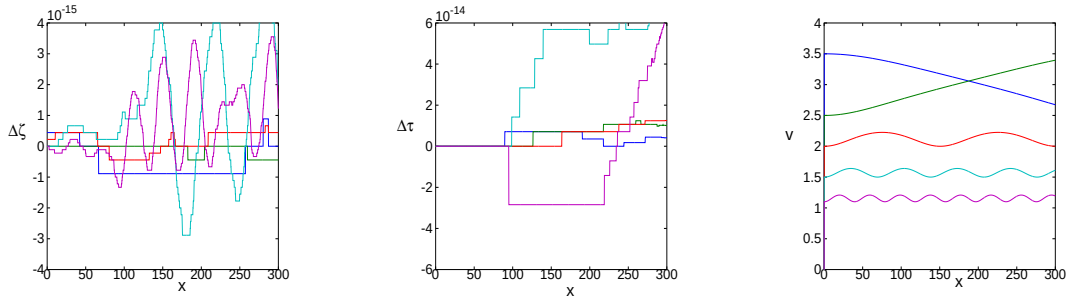


Figure 2: Discrepancy, between direct evolution $\mathcal{F}_{\Delta x}$ and backward evolution $\mathcal{F}^*_{-\Delta x}$, for energy (left panel) and arrival time (centre) as functions of position, for five particles in the field of a single wave with $A = 0.1$, $k = 0.2$, $v_\phi = 1$, $\phi = \pi$. Particles injected at the origin at $t = 0$, with velocities 1.1, 1.5, 2, 2.5 and 3.5, move as shown on right panel.

Finally the composition

$$\mathcal{F}^{(2)}_{\Delta x} = \mathcal{F}^*_{\Delta x/2} \circ \mathcal{F}_{\Delta x/2} = \mathcal{Z}^*_{\Delta x/2} \circ \mathcal{T}^*_{\Delta x/2} \circ \mathcal{I}_{\Delta x} \circ \mathcal{T}_{\Delta x/2} \circ \mathcal{Z}_{\Delta x/2} \tag{26}$$

is its own adjoint. It is thus symmetric and therefore second order [12].

## 4. Validation : particle dynamics in a single wave

We test our schemes with the time dependent potential of a wave

$$V(x,t) = A\cos(kx - kvt + \phi) \tag{27}$$

where $A, k, v, \phi$ are respectively the amplitude, wavevector, phase velocity and phase of the wave. Rescaling energy (and amplitude), space and time enables one to set $m$, $k$ and $v$ to unity, and the choice of the origin of time or space eliminates $\phi$. Its integrability makes this dynamics a good benchmark.

The accuracy of the determination of the adjoint map is checked by iterating first $\mathcal{F}_{\Delta x}$ for $\Delta x = 0.01$ from $x = 0$ to $x = L = 300$, and then $\mathcal{F}^*_{-\Delta x}$ from $x = L$ to $x = 0$, for five particles. Figures 2 display the discrepancies $\Delta\zeta$ and $\Delta\tau$ as functions of $x$ for each particle and confirm that $\mathcal{F}^*_{-\Delta x} = \mathcal{F}^{-1}_{\Delta x}$ to numerical accuracy. The order of the algorithms and their accuracy is further analysed in figure 3, comparing the first order and second order schemes for the motion of a particle with initial velocity $v_{\rm in} = 1.5$ in the field of a wave with $A = 0.1, \phi = \pi, k = 0.2, v_\phi = 1$ over a length $L = 100$.

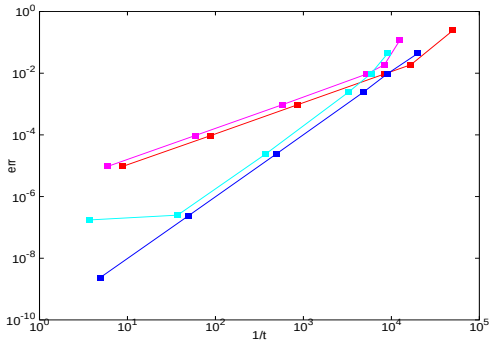


Figure 3: Numerical accuracy for the first order algorithm (red, upper lines) and second order (blue, lower lines) versus calculation time per spatial unit length. Darker colour for the Newton method solution to the cubic equation, lighter colour for polynomial solver (slightly slower than Newton).

## 5. Beam dynamics in a single wave

A second accuracy check is provided by the Poincaré section of the beam by the positions $x \bmod L = 0$. The return map for $(\tau, \zeta)$ variables is symplectic. As the particle motion is integrable (it reduces to the pendulum by a Galileo transformation to the reference frame comoving with the wave), each orbit must generate section points on lines satisfying the algebraic relation

$$\zeta = \frac{mv_\phi^2 + \bar{H}}{2} \pm v_\phi \sqrt{2m\bar{H} - 2mA\cos[k(x - v_\phi\tau) + \phi]} \tag{28}$$

where $\bar{H}$ is a constant. In particular, the motion on the wave separatrix corresponds to $\bar{H} = A$. For $\bar{H} > A$, this relation defines two branches for all times $\tau$, which correspond to faster or slower circulating particles, while for $\bar{H} < A$ the relation defines the upper and lower part of trapped motion inside the wave's cat eye. Figure 4 shows that numerical trajectories perfectly reproduce these lines.

To assess the relevance of the algorithm to experiment we also follow the deformation of a beam of electrons injected in a single wave, e.g. in a traveling wave tube. As particles are accelerated or decelerated by the wave, the beam velocity profile is deformed. We thus inject $N$ particles at $x = 0$, equally distributed over one time period of the wave, and plot the histogram of particle velocities as a function of abscissa $x$.

In figure 5 a cold beam is made of particles injected resonantly with the wave velocity, $v_\mathrm{b} = v_\phi = 1$, with $m = k = 1$. The wave amplitude, $A = 0.002$, determines

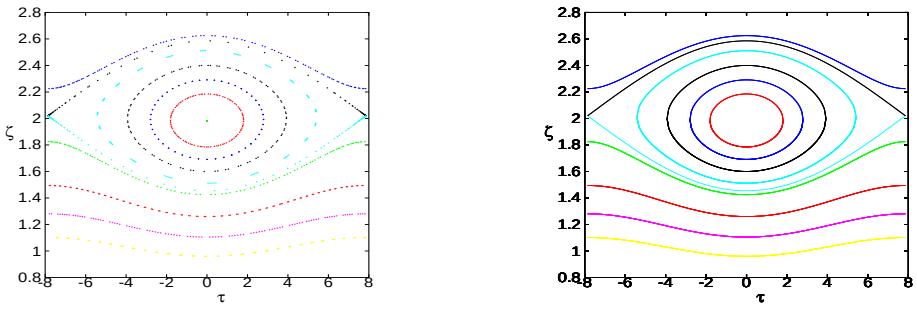


Figure 4: (left) Poincaré section in $(\tau, \zeta)$ variables, of the return map after one wavelength $L$. Trajectories for five trapped particles injected with $v_{\rm in} = 1.8, 1.85, 2, 2.1, 2.25$, for five untrapped particles with $v_{\rm in} = 1.4, 1.5, 1.6, 1.7, 2.3$, and for one particle injected on each separatrix branch. Wave parameters $A = 0.02, v_\phi = 2, k = 0.2, \phi = \pi$ ; particle mass $m = 1$. (right) Exact section lines (28).

the bounce frequency $\omega_{\rm b} = \sqrt{kA}$ so that particle oscillations in the wave trough have a spatial period $L_{\rm b} = 2\pi v_\phi/\omega_{\rm b} = 140.5$. The particles bounce indeed and, in agreement with the rotating bar approximation [17], most of them reconvene every $L_{\rm b}/2$. Only the ones injected at times close to $(\phi + 2\pi n)/(kv_\phi)$ (for integer $n$) enter the wave close to the X point and follow closely the inner side of the cat eye separatrix. The time these particles need to overcome half a wavelength can be arbitrarily long, so that they mark the boundary of the wave resonant domain at velocities $v_\phi \pm 2\sqrt{A/m}$.

For particles injected with a velocity outside the wave cat's eye, the beam is modulated. A significant difference between $(x, v)$ plots for propagating beams and the more familiar $(x, v)$ Poincaré sections of particle-in-wave dynamics (see e.g. [11, 10, 9]) is the asymmetry between faster and slower particles, obvious in Figure 6.

In particular, for particles injected with a velocity above the wave cat's eye, the beam is moderately asymmetric. But for a particle injection velocity within the capture range $[v_\phi - 2\sqrt{A/m}, v_\phi + 2\sqrt{A/m}]$, the picture gets strongly deformed, as part of the beam is trapped as in figure 5 while part of it moves outside the wave cat's eye.

## 6. Particle dynamics in two waves : resonance overlap and chaos

The motion of a particle in the field of two waves is a paradigm of hamiltonian chaos. In our formulation, Poincaré sections are given by $x \bmod L = 0$, and the return map is symplectic, hence area-preserving in conjugate variables $(\tau, \zeta)$. Figure 7 displays

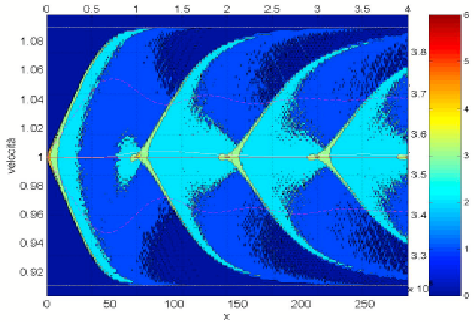

Figure 5: Velocity distribution function of particles along the $x$ axis, injected at the wave phase velocity, $v_\mathrm{b} = v_\phi = 1$, with $m = k = 1$ and wave amplitude $A = 0.002$.

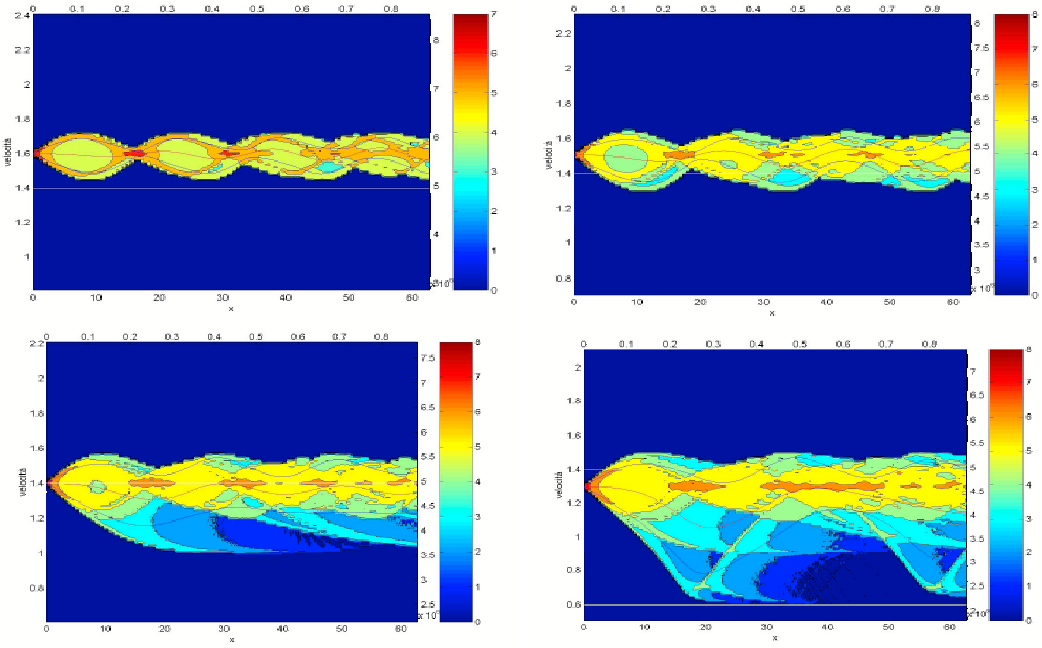

Figure 6: Velocity distribution function of particles along the $x$ axis, when injected at $v_\mathrm{b} = 1.6$ (upper left), $v_\mathrm{b} = 1.5$ (upper right), $v_\mathrm{b} = 1.4$ (lower left) and $v_\mathrm{b} = 1.3$ (lower right), above the wave phase velocity, $v_\phi = 1$, with $m = k = 1$ and wave amplitude $A = 0.04$. The cat's eye boundaries lie at $v_\phi + 2\sqrt{A} = 1.4$ and $v_\phi - 2\sqrt{A} = 0.6$.

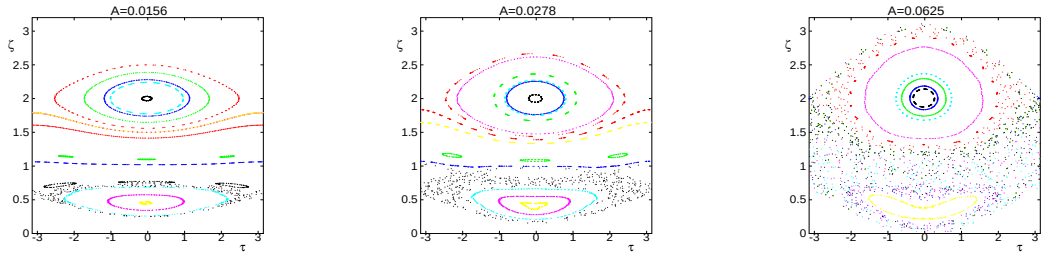


Figure 7: Poincaré section in $(\tau, \zeta)$ variables, of the return map after one wavelength $L$, for 15 particles, with mass $m = 1$. Wave parameters are $k_1 = 1$, $k_2 = 1/2$, $v_{\phi 1} = 1$, $v_{\phi 2} = 2$, $\phi_1 = \phi_2 = \pi$. Wave amplitudes $A_1 = A_2$ yield overlap parameter $s = 0.5$ (left), 0.66 (centre) and 1 (right).

this Poincaré section, showing the growth of the chaotic domain for increasing wave amplitudes, and the destruction of KAM tori [11].

The corresponding transition to large scale chaos by increasing the resonance overlap parameter $s = 2(\sqrt{A_1} + \sqrt{A_2})/(|v_{\phi 2} - v_{\phi 1}|\sqrt{m})$ is also observed by recording the particle velocities at a fixed traveled distance $L_0$, after being injected at a fixed velocity $v_{\rm in}$. As seen in figures 6, a cold beam injected in a wave cat's eye spreads over the velocity interval spanned by this cat eye, and if the beam is injected outside cat eyes it remains confined between the velocities of KAM tori on either side. Beam velocity spreading (also called heating) has been used to diagnose resonance overlap, and our numerical scheme is compared with experimental data [5] in figure 8.

Moreover, the transition to large scale chaos in phase space is known to occur stepwise. For increasing wave amplitudes, successive KAM tori get destroyed, so that the beam invades velocity domains resulting from the merging of capture regions corresponding to "secondary" resonances [11]. The accessible velocity interval for the beam injected in one wave then grows like a devil's staircase, the higher steps corresponding to the merging with major secondary resonances. Figure 9 compares these domains obtained both numerically and experimentally [16, 7, 3]. While experimental data are blurred due to recording accuracy, numerical data have limited resolution due to the large number of particles (here only 25000) needed for the sharp observation of a threshold. Nevertheless, the agreement is quantitatively satisfactory.

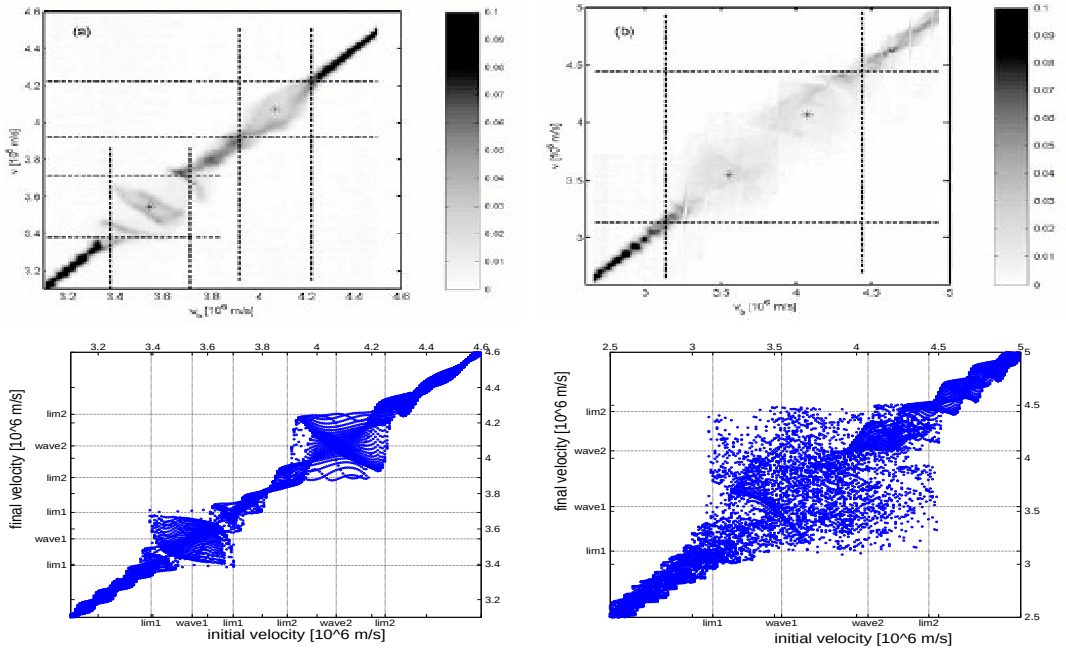


Figure 8: Velocities of particles after interaction with two waves, versus injection velocity. (top) Experimental data with dotted lines marking cat eyes boundaries ; (bottom) numerical results. (left) Non-overlapping cat eyes, $s = 0.63$ ; (right) overlapping trapping domains, $s = 1.5$.

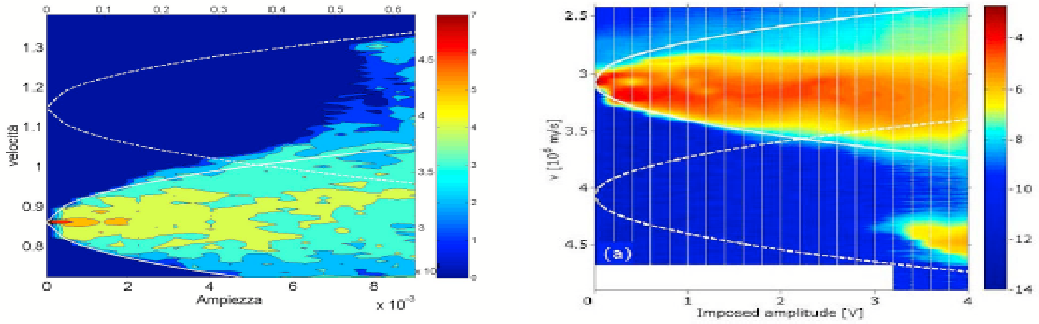


Figure 9: Velocities of particles after interaction with two waves, versus amplitude of waves $A_1 = A_2$. Cold beam injected at phase velocity of one wave. (left) Numerical results for $v_\mathrm{b} = v_{\phi 1} = 1.1487$, $v_{\phi 2} = 0.8609$, $k_1 = 0.6529$, $k_2 = 1.7424$. (right) Experimental data.

## 7. Conclusion

The scheme has proved its relevance to describe accurately particle motion in a given field, along a single space dimension. It also provides new pictures of known behaviours, which complement more familiar, usually more symmetric plots in $(x, v)$ space.

Extending our approach to three space dimensions is rather straightforward provided the particles stream along a given coordinate, say $x$. Higher-order symplectic schemes can also be constructed by composing several maps $\mathcal{F}_{\gamma_i \Delta x}$ and $\mathcal{F}^*_{\gamma_i \Delta x}$ with appropriate substeps $\gamma_i$ [12]. More challenging is the issue raised by the particle feedback on the wave field, calling for a self-consistent space-based model of particles and waves evolution, in the spirit of models used for weak plasma turbulence [9].

It will also be interesting to apply this scheme to model the many-waves regime of weak plasma turbulence, where particle velocity undergoes a chaotic transport over a wide range [4, 1, 9, 8, 2], as properties of this transport are still controversial.

## 8. Acknowledgements

The work of A. Ruzzon was made possible by an Erasmus mobility from Università degli studi di Padova to université de Provence. This work benefited from fruitful discussions with D.F. Escande.

## Appendix A. Explicit derivation of (17)

To reduce (16) to (17), note that the derivatives of momentum (11) read

$$\partial_\zeta \mathcal{P}(\tau, \zeta, x) = m\mathcal{P}^{-1}\,, \tag{A.1}$$

$$\partial_\tau \mathcal{P}(\tau, \zeta, x) = -m\mathcal{P}^{-1}\partial_\tau V\,, \tag{A.2}$$

and consider the dimensionless (both physically and numerically relevant) quantity $\sigma = (\tilde{\zeta} - \zeta)/(\zeta - V)$, which characterizes the changes in particle energy per step and must be small for an accurate calculation.

Equation (14) reads, with arguments $(\tau, \tilde{\zeta}, x)$ in $\mathcal{P}$ and $(\tau, x)$ in $V$,

$$\sigma = -\partial_\tau \mathcal{P}\Delta x/(\zeta - V) \tag{A.3}$$

$$= -\sqrt{\frac{m}{2}}\,\partial_\tau V \Delta x\,(\tilde{\zeta} - V)^{-1/2}(\zeta - V)^{-1} \tag{A.4}$$

$$= -a\left(\frac{\tilde{\zeta}-V}{\zeta-V}\right)^{-1/2} \tag{A.5}$$

$$= -a\left(1+\frac{\tilde{\zeta}-\zeta}{\zeta-V}\right)^{-1/2}, \tag{A.6}$$

using the dimensionless $a$ defined by (18). The fixed point equation (17) then follows.

## Appendix B. Explicit flowchart of the second order algorithm

The symmetric scheme (26) may be expanded as follows:

- $(\tau,\zeta,x)\mapsto(\tau,\zeta^*,x)$ : solve $\zeta=\zeta^*+\partial_\tau\mathcal{P}(\tau,\zeta^*,x)\Delta x/2$ for $\zeta^*$ ;
- $(\tau,\zeta^*,x)\mapsto(\tau^*,\zeta^*,x)$ : $\tau^*=\tau+\partial_\zeta\mathcal{P}(\tau,\zeta^*,x)\Delta x/2$ ;
- $(\tau^*,\zeta^*,x)\mapsto(\tau^*,\zeta^*,\tilde{x})$ : $\tilde{x}=x+\Delta x$ ;
- $(\tau^*,\zeta^*,\tilde{x})\mapsto(\tilde{\tau},\zeta^*,\tilde{x})$ : solve $\tau^*=\tilde{\tau}-\partial_\zeta\mathcal{P}(\tilde{\tau},\zeta^*,\tilde{x})\Delta x/2$ for $\tilde{\tau}$ ;
- $(\tilde{\tau},\zeta^*,\tilde{x})\mapsto(\tilde{\tau},\tilde{\zeta},\tilde{x})$ : $\tilde{\zeta}=\zeta-\partial_\tau\mathcal{P}(\tilde{\tau},\zeta^*,\tilde{x})\Delta x/2$.

## References


[1] D. Bénisti and D.F. Escande, Origin of diffusion in Hamiltonian dynamics, *Phys. Plasmas* **4** (1997) 1576–1581.

[2] N. Besse, Y. Elskens, D.F. Escande and P. Bertrand, Validity of quasilinear theory : refutations and new numerical confirmation, *Plasma Phys. Control. Fus.* **53** (2011) 025012.

[3] M. Buchanan, Richness in simplicity, *Nature Physics* **2** (2006) 429.

[4] J.R. Cary, D.F. Escande and A.D. Verga, Non quasilinear diffusion far from chaotic threshold, *Phys. Rev. Lett.* **65** (1990) 3132–3135.

[5] F. Doveil, Kh. Auhmani, A. Macor and D. Guyomarc'h, Experimental observation of resonance overlap responsible for Hamiltonian chaos, *Phys. Plasmas* **12** (2005) 010702.

[6] F. Doveil, Y. Elskens and A. Ruzzon, Observation and control of hamiltonian chaos in wave-particle interaction, in : A. Sen, S. Sharma and P.N. Guzdar (Eds), *International symposium on waves, coherent structures and turbulence in plasmas* (Gandhinagar, 2010), *AIP Proc.* **1308** (2010) 132–141.

[7] F. Doveil, A. Macor and Y. Elskens, Direct observation of a "devil's staircase" in wave-particle interaction, *Chaos* **16** (2006) 033103.

[8] Y. Elskens, Nonquasilinear evolution of particle velocity in incoherent waves with random amplitudes, *Commun. Nonlinear Sci. Numer. Simul.* **15** (2010) 10–15.

[9] Y. Elskens and D. Escande, *Microscopic dynamics of plasmas and chaos* (Bristol: IoP Publishing, 2003).

[10] D.F. Escande, Stochasticity in classical hamiltonian systems : universal aspects, *Phys. Rep.* **121** (1985) 165–261.

[11] D.F. Escande and F. Doveil, Renormalization method for the onset of stochasticity in a hamiltonian system, *Phys. Lett. A* **83** (1981) 307–310.

[12] E. Hairer, C. Lubich and G. Wanner, *Geometric numerical integration : Structure-preserving algorithms for ordinary differential equations* (New York: Springer, 2002).

[13] M. Hénon, On the numerical computation of Poincaré maps, *Physica D* **5** (1982) 412-414.

[14] M.V. Kartikeyan, E. Borie and M.K.A. Thumm, *Gyrotrons – High power microwave and millimeter wave technology* (Berlin: Springer, 2004).

[15] B. Leimkuhler and S. Reich, *Simulating hamiltonian dynamics* (Cambrige: University press, 2005).

[16] A. Macor, F. Doveil and Y. Elskens, Electron climbing a "devil's staircase" in wave-particle interaction, *Phys. Rev. Lett.* **95** (2005) 264102.

[17] H.E. Mynick and A.N. Kaufman, Soluble theory of nonlinear beam-plasma interaction, *Phys. Fluids* **21** (1978) 653–663.

[18] A. Ruzzon, *Studio numerico della propagazione spaziale d'un fascio di test in un tubo a onde progressive e confronto con l'esperimento* (tesi di laurea, Università degli studi di Padova, Padua, 2009).